GEOFLUIDS

Geofluids (2014) **14**, 174–188 doi: 10.1111/gfl.12061

Fluid effect on hydraulic fracture propagation behavior: a comparison between water and supercritical CO_2-like fluid

X. ZHOU[1,2] AND T. J. BURBEY[1,2]

[1]*National Energy Technology Laboratory—Regional University Alliance (NETL-RUA), Pittsburgh, PA, USA;* [2]*Department of Geosciences, Virginia Tech, Blacksburg, VA, USA*

ABSTRACT

The initiation of hydraulic fractures during fluid injection in deep formations can be either engineered or induced unintentionally. Upon injection of CO_2, the pore fluids in deep formations can be changed from oil/saline water to CO_2 or CO_2 dominated. The type of fluid is important not only because the fluid must fracture the rock, but also because rocks saturated with different pore fluids behave differently. We investigated the influence of fluid properties on fracture propagation behavior by using the cohesive zone model in conjunction with a poroelasticity model. Simulation results indicate that the pore pressure fields are very different for different pore fluids even when the initial field conditions and injection schemes (rate and time) are kept the same. Low viscosity fluids with properties of supercritical CO_2 will create relatively thin and much shorter fractures in comparison with fluids exhibiting properties of water under similar injection schemes. Two significant times are recognized during fracture propagation: the time at which a crack ceases opening and the later time point at which a crack ceases propagating. These times are very different for different fluids. Both fluid compressibility and viscosity influence fracture propagation, with viscosity being the more important property. Viscosity can greatly affect hydraulic conductivity and the leak-off coefficient. This analysis assumes the in-situ pore fluid and injected fluid are the same and the pore space is 100% saturated by that fluid at the beginning of the simulation.

Key words: cohesive finite element method, cohesive zone model, fracture propagation, hydraulic fracture, pore fluid

Received 21 January 2013; accepted 11 August 2013

Corresponding author: Xuejun Zhou, Department of Geosciences, Virginia Tech, 1425 Perry St., Blacksburg, VA, 24061 USA.
Emails: zhouxj@vt.edu, zhxjun@yahoo.com. Tel: 540 231 2404. Fax: 540 231 3386.

Geofluids (2014) **14**, 174–188

INTRODUCTION

A particular class of fractures in the earth develops as a result of internal pressurization by a fluid (Detournay 2004). Dykes and sills are natural examples of hydraulically induced fractures (Pollard 1976; Spence & Turcotte 1985), whereas hydraulic fractures designed to increase oil/gas production are man-made and have been used to stimulate over 70% of gas wells and 50% of oil wells in North America in the last half-century (Economides & Nolte 2000). Other applications include preconditioning of ore bodies, disposal of waste drill cuttings, remediation of contaminated land, and measurement of in-situ stress (Haimson & Fairhurst 1969; Sun 1969; Zoback *et al.* 1977; Evans *et al.* 1999; Murdoch & Slack 2002; Haimson & Cornet 2003; Frank & Barkley 2005; Legarth *et al.* 2005; Adachi & Detournay 2008).

Carbon dioxide has been used as a liquefied gas in oil and gas field stimulation since the early 1960s because it eliminates formation damage and residual fluids (Harris *et al.* 1984; Sinal & Lancaster 1987). Carbon dioxide injection is considered one of the most effective technologies for improving oil recovery from hard-to-extract oil reserves because CO_2 is effective in penetrating the formation due to its high diffusivity, and the rock associated with petroleum-containing formations is generally porous (Fink 2011). Field experience in petroleum engineering indicates that different fracturing fluids can result in different patterns of fracture creation and propagation. Viscous fluids tend to generate thick and planar cracks with few branches, while thin or low viscosity fluids tend to generate narrow and wavelike cracks with many secondary branches (Ishida *et al.* 1998, 2004). Even liquid CO_2 and supercritical CO_2 show different fracturing features in a

recent laboratory test, with supercritical CO_2 generating cracks that extend much more three-dimensionally (Ishida *et al.* 2012). Some field experiences also show that when other normally used hydraulic fluids can fracture the formation at a comparable injection flow rate, CO_2 cannot (Yao 2012).

Two energy dissipation mechanisms and two fluid storage mechanisms compete during hydraulic fracturing. The energy dissipation mechanisms are mainly related to viscous flow and the creation of fracture area in solid host rock. The fluid storage mechanisms are storage of fluid in the fracture and leak-off of fluid into the permeable solid. These two sets of mechanisms are associated with four combined asymptotic regimes: storage-toughness (Garagash 2006), storage-viscosity (Savitski & Detournay 2002), leak-off-toughness (Bunger *et al.* 2005), and leak-off-viscosity (Adachi & Detournay 2008). For example, the toughness-dominated regime refers to a condition of large toughness or, equivalently, a low fracturing fluid viscosity. Here, toughness refers to how easy or difficult it is for a fracture to be initiated and/or propagated within a formation. In such a regime, the energy dissipated by viscous fluid flow inside the fracture is negligibly small compared to the energy expended in fracturing the solid medium. On the vertex of storage-viscosity-dominated regime, fluid leak-off is negligible compared to fluid storage in the fracture and the energy expended in fracturing the rock is negligible compared to viscous dissipation (Garagash 2006; Peirce & Detournay 2008a,b).

The relative magnitude of the dissipation processes on one hand, and of the storage processes on the other hand, can be described by a dimensionless toughness K' and a dimensionless leak-off coefficient C' (Adachi & Detournay 2008; Carrier & Granet 2012), respectively:

$$K' = \frac{4K_{IC}}{\sqrt{\pi}}\left(\frac{1}{3Q_0E'^3\mu}\right)^{1/4};\ C' \approx 2\frac{\kappa}{\mu}\frac{\sigma_0}{\sqrt{\pi c}}\left(\frac{E't}{12\mu Q_0^3}\right)^{1/6} \quad (1)$$

where K_{IC} is fracture toughness, E' is dimensionless Young's modulus, c is diffusivity coefficient, Q_0 is injection rate, μ is fluid viscosity, σ_0 is the confining stress, κ is the intrinsic permeability and related with the hydraulic conductivity k by $\kappa = k\mu/\rho_f g$, ρ_f is fluid density. Here, viscosity (or a power of it) is inversely related to K' and C' in both equations. Figure 1 shows the two-dimensional parameter space of dimensionless toughness K' and dimensionless leak-off coefficient C'. Each edge of this space represents an asymptotic regime. During the injection of fluid into a plane strain fracture, the propagation regime evolves from storage-dominated to leak-off-dominated with time (Carrier & Granet 2012).

A supercritical fluid exhibits physiochemical properties intermediate between those of liquids and gases. Mass transfer is rapid with supercritical fluids because their

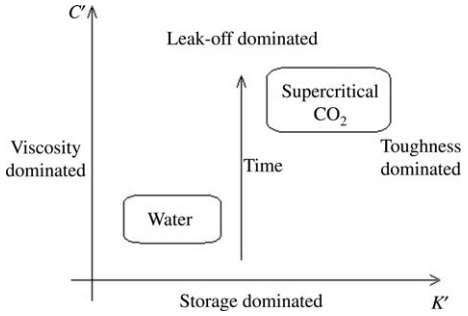

Fig. 1. Schematic hydraulic fracture parametric space with respect to different fluids (water and supercritical CO_2).

dynamic viscosities are nearer to those of normal gaseous states. The K' and C' values when supercritical CO_2 is injected will be much larger than those of water because supercritical CO_2 has a much smaller viscosity than water; μ_{CO_2} is in the range of 0.02~0.16 cp (Fenghour *et al.* 1998; Heidaryana *et al.* 2011), while μ_{HO_2} is about 1 cp. The relatively large K' and C' values will tend to put injection of supercritical CO_2 closer to the leak-off-toughness-dominated regime than injection of water.

The pore fluids in deep formations will be changed from one type of fluid to another after consistent fluid injection, and rock formations saturated with such different pore fluids will behave very differently. Water-/oil-saturated rock and CO_2-saturated rock will have very different pore pressure change curves because of their different Skempton's B values, and consequently, the fractures may propagate very differently (Berryman 2012). The objective of this paper is to investigate the effect of fluid properties on hydraulically induced fracture propagation behavior by using the cohesive finite element method (CFEM) or cohesive zone modeling approach.

In this paper, we focus on the effect of a fluid's hydro-mechanical properties on the hydraulic fracture's propagation behavior and assume single-phase flow conditions, that is, the in-situ pore fluid and the injected fluid are the same and the pore space is 100% saturated by that fluid at the beginning of the simulation. A single phase analysis using either supercritical CO2 or water allows us to make an end-member comparison of the hydro-mechanical effects of these fluids on the fracture initiation/propagation behavior during fluid injection.

THE COHESIVE ZONE MODEL

Due to the difficulty of making accurate measurements of the fracture geometry during and after the hydraulic fracturing, modeling of the process assumes special importance (Adachi 2001). However, hydraulic fracturing is not a trivial process to model as it involves the coupling of several physical processes with singular behavior at the fracture tip

(Sarris & Papanastasiou 2011). The cohesive zone model allows explicit modeling of fracturing in monolithic and composite material systems. The cohesive zone model in its infancy was described by Barenblatt's 'cohesive force' model (1959, 1962), Dugdale's 'strip-yield' model (1960), and Hillerborg's 'fictitious crack model' (Hillerborg *et al.* 1976). Cohesive zone elements do not represent any physical material, but describe the cohesive forces that occur when materials are being pulled apart. A series of investigations have been conducted dealing with the development of computational fracture mechanics (Camacho & Ortiz 1996; Needleman 1987; Falk *et al.* 2001; etc.) and hydraulic fracturing (Boone *et al.* 1986; Boone & Ingraffea 1990; Papanastasiou & Thiercelin 1993; etc.).

In classic linear elastic fracture mechanics (LEFM), an elastic crack tip region has an infinite stress at the sharp crack tip. The cohesive zone model assumes a fracture process zone characterized by a traction–separation law to avoid the singularity in the crack tip stress field that is present in classic fracture mechanics. The ability of a cohesive zone model to simulate a hydraulic fracture in different propagation regimes, such as the toughness-dominated and viscosity-dominated regimes, has been demonstrated by the work of Chen *et al.* (2009), Carrier & Granet (2012) and Chen (2012), etc.

The success of this approach may lie in the assumption that the stress-intensity factors at the crack tip are extremely small, and the limit of zero is perhaps the most common case (Spence & Sharp 1985; Spence & Turcotte 1985). Laboratory tests have also found that the viscosity-dominated regime prevails during hydraulically driven crack propagation in many real world conditions, with the crack tip effect extremely small in comparison with the dimension of the crack (Bunger & Detournay 2008). The cohesive zone model is more suitable for crack problems than LEFM for cemented materials because the size of the nonlinear zone is not negligible, due for instance to plasticity or micro-cracking. In fact, many hydraulic fracturing operations are performed in relatively 'soft' formations, such as porous sedimentary rocks (limestone or sandstone) or shale (impermeable but weak rock) instead of hard igneous rocks (granite) that are prone to nonlinear failures, which differ from LEFM (Elices *et al.* 2002; Adachi *et al.* 2007).

Figure 2 shows a cohesive zone model under tension failure due to a forced incoming fluid. The fluid flows in the cohesive zone with leak-off into the surrounding porous formation. The fluids can be separated into tangential flow and normal flow, and the fluid leak-off effect is defined by a permeable layer (Fig. 2). Leak-off from the fracture into the formation and pore pressure diffusion may change effective stresses in the formation and hence the size of the plastic zones (Papanastasiou 1999). The influence of fluid leak-off and pore pressure in a stationary hydraulic fracture in a poroelastic medium has been investigated by Detournay & Cheng (1991).

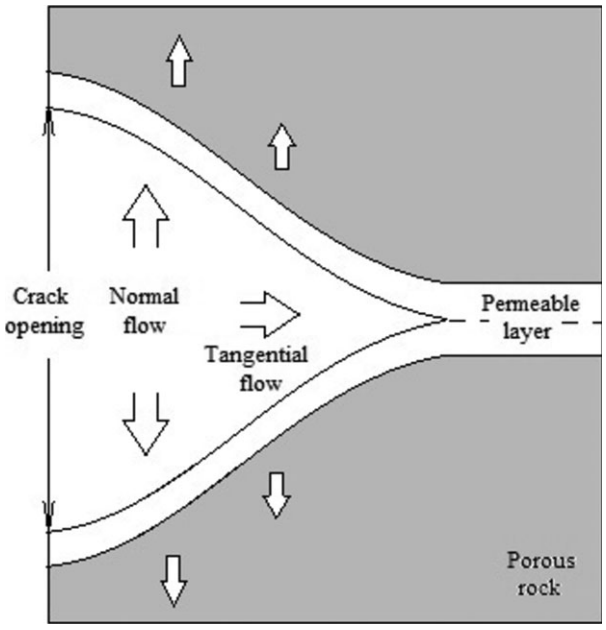

Fig. 2. Fluid flow in a cohesive zone with leak-off.

Figure 3 shows the schematic constitutive cohesive law for a typical cohesive traction–separation curve (Shet & Chandra 2002) and its linear and exponential approximations. The constitutive behavior of the cohesive zone is based on laboratory tests. The traction–separation constitutive relation for the surface is such that with increasing separation, the traction across a pair of cohesive surfaces reaches a peak and then decreases (either linearly or exponentially) and eventually vanishes to permit a complete separation.

GOVERNING EQUATIONS

The consideration of hydraulically induced fractures is at the juncture of four classical disciplines: lubrication theory, filtration theory, fracture mechanics, and poroelasticity. This type of problem involves the coupling of four distinct processes: (i) the relationship between fracture opening and the incoming fluid; (ii) the flow of fluid within the fracture; (iii) the propagation of the fracture; and (iv) leak-off of the fracturing fluid into the permeable medium, which is a time-dependent process (Bunger *et al.* 2005; Adachi & Detournay 2008). The equations governing the propagation of a hydraulic fracture in a reservoir have to account for these four dominant physical processes in addition to the deformation of the rock, the creation of new fracture surfaces, and fluid diffusion in the reservoir (Peirce & Detournay 2008b).

This paper considers the plane strain problem of a hydraulic fracture propagating in a permeable and linear

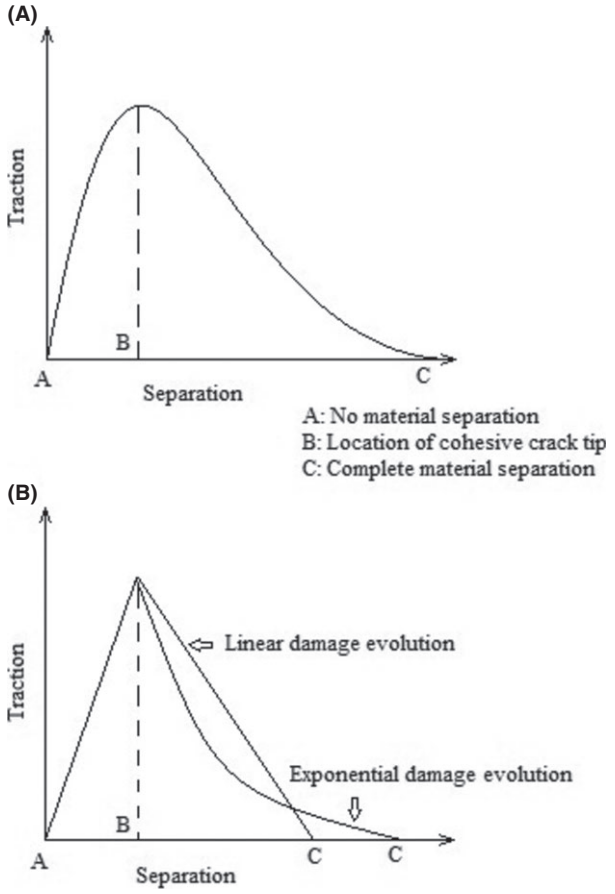

Fig. 3. Constitutive cohesive law (A) a typical cohesive traction–separation curve under stain control (B) linear and exponential approximations.

elastic medium. The particular problem of interest is conceptualized in plane strain and is usually referred to as a KGD fracture (in honor of Khristianovitch, Geertsma and de Klerk) (Geertsma & de Klerk 1969). The symmetry of the problem allows us to model only half of the space. The *x*-axis coincides with the fracture path with its origin at the injection point (Fig. 4).

Fracture propagation theory based on cohesive law

The cohesive zone represents a region ahead of the crack tip and is characterized by microcracking along the crack path (Sarris & Papanastasiou 2011). The progressive damage and failure in cohesive layers is defined in terms of traction–separation law, in which a cohesive potential function ψ can be expressed as a function of the traction tensor T and the displacement jump Ω across a pair of cohesive surfaces (Chen 2012):

$$\partial\psi = T \bullet \partial\Omega \tag{2}$$

The cohesive zone model implies that normal stress continues to be transferred across a discontinuity and is a

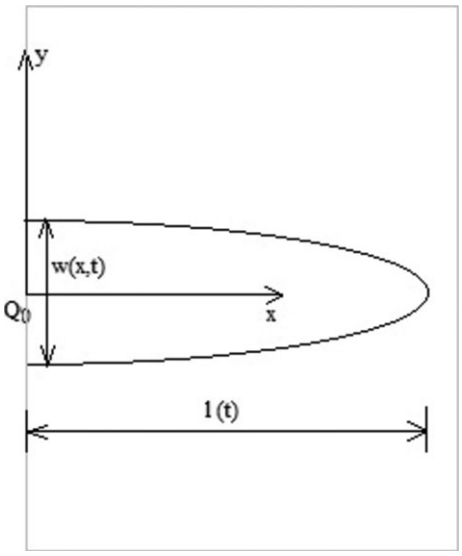

Fig. 4. KGD fracture problem.

function of the separation, falling to zero at a critical opening at which point the fracture propagates. During hydraulic fracturing, the fluid pressure is considered as traction acting on the open surfaces of the fracture and is balanced by the far-field stress and by the cohesive tractions acting across the cohesive zone. The traction tensor T relates to the field pore pressure (p_∞) (the pore pressure with enough distance from the fracture thus can be considered as a reference state without the disturbance of fluid injection), injection pressure inside of the fracture (p_i), and confining stress tensor σ_{ij} for a tensile failure criterion in the normal direction:

$$T = \sigma_{ij} - \delta_{ij}(p_\infty + \Delta p_i), \quad T \le T_{\max}; \quad \Delta p_i = p_i - p_\infty \tag{3}$$

where δ_{ij} is the Kronecker delta. This equation shows that the traction will decrease when pore pressure increases within the cohesive zone during fluid injection. The tensile strength comes into play once the injection pressure is higher than the confining stress, and tensile failure will be initiated once a tensile threshold is exceeded. The traction will eventually recover to equal to the far-field effective stress after pumping stops, and the fracture will finally close except where the opening is sustained by particles introduced during the fracturing process.

Hydraulic fracture modeling based on cohesive zone model requires fracture toughness as the fracture initiation criterion, which is a quadratic nominal stress criterion of the cohesive finite element method used in this paper (Hibbitt, Karlsson & Sorensen, Inc. 1998). In this criterion, damage is assumed to initiate when a quadratic interaction function involving the nominal stress ratios reaches unity:

$$\left[\frac{t_n}{t_n^{\max}}\right]^2+\left[\frac{t_{s1}}{t_{s1}^{\max}}\right]^2+\left[\frac{t_{s2}}{t_{s2}^{\max}}\right]^2=1 \tag{4}$$

where t_n and t_{s1}, t_{s2} are the normal, the first and second shear tractions, respectively. Because shear tractions are very small in our hydraulic fracturing problem configuration, fracture initiation will mainly be determined by the normal traction maximum $t_n^{\max}$. Note that the maximum cohesive traction tensor T_{max} is related to these tractions by $T_{\max}=t_n^{\max}, t_{s1}^{\max}, t_{s2}^{\max}$. Various types of traction–separation relations for the cohesive zone model have been proposed for fracture propagation, and the bilinear model is generally considered a good choice due to its straightforward physical background (Tomar *et al.* 2004). For a pure normal deformation mode, the cohesive energy G_c, the maximum cohesive traction tensor T_{max}, and the critical separation at complete failure Ω_f are related through the following function (Chen 2012):

$$G_C=\frac{1}{2}T_{\max}\Omega_f \tag{5}$$

Fluid flow in the fracture

The injection rate of an incompressible fluid into a fracture in a plane strain configuration having an infinite permeable medium is assumed to be a constant Q_0. Note that at very high pore pressures, even supercritical CO_2 can be so-considered for purposes of this problem. The mathematical model that describes the propagation of a fracture of half-length $l(t)$ and aperture $w(x,t)$ (Fig. 4) through an infinite poroelastic medium begins with global conservation of fluid injected at the crack inlet V_{inject} (Bunger *et al.* 2005):

$$V_{inject}=\frac{Q_0 t}{2}=V_{crack}+V_{leak} \tag{6}$$

The volumes of the fluid stored in the crack V_{crack} and leaked into the porous solid V_{leak} are correspondingly:

$$\begin{aligned} V_{crack}&=\int_0^{l(t)} w(x,t)dx, t>0\\ V_{leak}&=\int_0^t dt'\int_0^{l(t')}\frac{2C}{\sqrt{t-t_0(x)}}dx, t-t_0(x)>0 \end{aligned} \tag{7}$$

where C is the leak-off parameter characterizing the loss of fluid into the solid material, t_0 is the lapse time since the exposure of the fracture surface to the fluid. The local fluid flux $Q(t)\delta(x,y)$ is the summation of the tangential flux $\nabla\cdot q_T$ and the normal flux $\nabla\cdot q_N$ with the consideration of aperture change based on local mass conservation (Savitski & Detournay 2002; Peirce & Detournay 2008a).

$$Q(t)\delta(x,y)=\frac{\delta_w}{\delta_t}+\nabla\cdot q_T+\nabla\cdot q_N \tag{8}$$

Lubrication theory is used to model the flow of fluid within the crack. If the fluid is assumed to have Newtonian rheology within the crack and the crack is such that $w/l\ll 1$, then the tangential flow q_T in the fluid-filled part of the fracture is governed by Poiseuille's law:

$$q_T=-\frac{w^3}{12\mu}\nabla p \tag{9}$$

where μ is fluid viscosity, and ∇p is the pore fluid gradient along the central line of the fracture. The normal flow q_N can be defined as:

$$q_N=2C(p_C-p_b) \tag{10}$$

where p_c is the pore pressure on the central line of the fracture with $p_c\approx p_i$ because the pressure gradient of fluid within the fracture is much smaller than the difference between p_c and p_b. Here, p_b is the pore pressure on the fracture boundary, assuming a symmetric configuration such that the upper and the lower boundary conditions do not differ.

Poroelasticity field equations

Poroelastic effects have been ignored when modeling hydraulic fractures in many works in the past. However, poroelastic effects can be significant if the rock is considered to be porous. Modeling the poroelastic effect in hydraulic fracturing was pioneered by Cleary in the form of a back-stress (Cheng *et al.* 1993; Cheng & Detournay 1998). A hydraulic fracture in a poroelastic medium represents a (changing) surface across which the solid displacement and the normal fluid flux are discontinuous (Detournay *et al.* 1990; Detournay & Cheng 1991). As a starting point, the general constitutive equations for a continuous porous field govern both the deformation of the elastic porous medium and the diffusion of fluid through the pore space of the material (Rice & Cleary 1976; Berryman & Milton 1991):

$$\sigma_{ij}=2G\left(\varepsilon_{ij}+\frac{v}{1-v}\varepsilon_{ij}\delta_{ij}\right)-2\eta\frac{1-v}{1-2v}p_\infty\delta_{ij} \tag{11}$$

$$\Delta m_f=\frac{\rho_f(1-v)}{G(1+v)}\eta\left(\sigma_{kk}+\frac{3}{B}p_\infty\right) \tag{12}$$

$$\eta=\frac{3(v_u-v)}{2B(1-v)(1+v_u)} \tag{13}$$

$$B=\frac{\frac{1}{K}-\frac{1}{K_s}}{\frac{1}{K}-\frac{1}{K_s}+n\left(\frac{1}{K_f}-\frac{1}{K_u}\right)} \tag{14}$$

where η is an intermediate parameter as defined by Eqn. 13. B is Skempton's B coefficient and is defined by Eqn. 14, σ_{ij} and ε_{ij} are stress and strain tensors, respectively, v_u and v are undrained and drained Poisson's ratio, respectively, n is porosity, G is shear modulus, p_∞ is field

pore pressure, ρ_f is fluid density, K is drained bulk modulus, K_s is bulk modulus of the solid grains, $1/K_n$ is the unjacketed pore compressibility, and K_f is the pore fluid bulk modulus. Pore fluid mass change Δm_f in the porous formation is related to the normal flow through the fracture by the equation:

$$\Delta m_f = \rho_f V_{leak} = \rho_f \int_0^t dt' \int_0^{l(t')} \frac{2C}{\sqrt{t - t_0(x)}} dx, t - t_0(x) > 0 \tag{15}$$

where ρ_f is fluid density, V_{leak} refers to the fluid volume that leaked into the porous solid, C is leak-off coefficient. Next, consider fluid flow field outside of the fracture where the behavior of the fluid leaking off into the porous formation is controlled by the pore pressure gradient and the compressibility of fluid as well as the mobility of the fluid. Due to the pore pressure gradient between the fracture zone and the far-field, a groundwater flow equation can be written with the addition of a term that incorporates stress effects on the pore pressure (Renshaw & Harvey 1994). The fundamental governing equation for transient flow is derived by combining Darcy's Law and the conservation of fluid mass (Green & Wang 1990):

$$\nabla^2 h = \frac{S_s}{k}\frac{\partial h}{\partial t}; \quad S_s = g\frac{\partial m_f}{\partial p}; \quad \frac{\partial m_f}{\partial t} = \rho_f S_s \frac{\partial h}{\partial t} \tag{16}$$

where h is hydraulic head, S_s is the specific storage coefficient, k is the hydraulic conductivity ($k = \kappa\rho_f g/\mu$), m_f is the fluid mass, and dp refers to the differential pressure between p_∞ (field pore pressure) and p_b (fluid pressure at fracture boundary). For the commonly applied boundary conditions of constant horizontal aquifer strain $\Delta\varepsilon_{11} = \Delta\varepsilon_{22} = 0$ and constant overburden ($\Delta\sigma_{33} = 0$), specific storage coefficient can be derived as (Green & Wang 1990):

$$\begin{aligned} S_s &= g\frac{dm_f}{dP}\bigg|_{\Delta\sigma_{33}=0;\Delta\varepsilon_{11}=\Delta\varepsilon_{22}=0} \\ &= \rho_f g\left\{\left[\left(\frac{1}{K}-\frac{1}{K_s}\right)+n\left(\frac{1}{K_f}-\frac{1}{K_s}\right)\right]-\frac{4\alpha}{3}G\left(1-\frac{K}{K_s}\right)\left(\frac{1}{K}-\frac{1}{K_s}\right)\right\} \end{aligned} \tag{17}$$

where K is drained bulk modulus of the porous material, K_s is bulk modulus of the solid grains, K_f is bulk modulus of the pore fluid, G is shear modulus, α is the compressibility along the vertical direction.

The fluid leak-off into the formation is dependent on the fracturing pressure, with the leak-off velocity v_l expressed as (Abousleiman 1991):

$$v_l = \frac{\kappa}{\mu\sqrt{\pi c}}\left(\frac{\sigma_0 - p_\infty}{\sqrt{t_0}} + \int_0^{t_0} \frac{\partial p_i}{\partial t}\frac{1}{\sqrt{t_0 - t}} dt\right) \tag{18}$$

$$c = \frac{2\kappa B^2 G(1-\nu)(1+\nu_u)^2}{9\mu(1-\nu_u)(\nu_u-\nu)} \tag{19}$$

where t_0 is the lapse time since the exposure of the fracture surface to the fluid, κ is intrinsic permeability, G is shear modulus, B is Skempton's B coefficient, and c is the diffusivity coefficient. It has been demonstrated that the time scale of the diffusional process in poroelasticity is controlled by the diffusivity coefficient (Green & Wang 1990; Cheng *et al.* 1993). The effects of fluid properties can be demonstrated by the parameters μ, B, K_f, c, ρ_f in these equations.

A multiphase flow condition arises if the injected fluid is different from the pore fluid, and new equations such as the Buckley-Leverett equation may be introduced (Pinder & Gray 2008), which is beyond the scope of this paper.

NUMERICAL SIMULATION

In this paper, calculations were carried out using the software platform Abaqus, a finite element code with a cohesive element function. Abaqus is also capable of simulating poroelasticity problems where the drained bulk moduli of both solid matrix and saturated pore fluid are dependent on the pore pressure (Schoenball *et al.* 2010).

The model for evaluating fracture formation and propagation

Figure 5 shows the discretized domain area of 100 × 100 m. The cohesive finite element is generally taken as a very thin layer (on the order of 0.1 mm or even less). The element spacing adjacent to a cohesive element should also be very fine in order to accurately simulate the

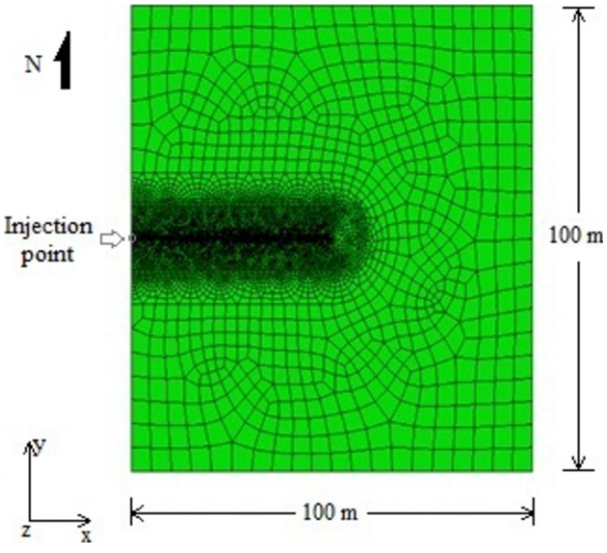

Fig. 5. Mesh layout of the model.

fracture propagation profile. Consequently, an extremely large number of elements are required for a model of significant size because of the intention to also consider the far-field effects. Eight nodes are required for a normal cubic element, and for a cohesive element, 12 nodes are required because four nodes are needed in the middle for the fluid flow calculation. The z-dimension thickness of the model is 1 m. The cohesive zone representing the predefined path of the fracture is 50 m long and the mesh in that region is very fine. Close to the cohesive zone, meshes with similar sizes are preferable as they can minimize mesh-induced dispersion effects in stress wave propagation (Falk *et al.* 2001). The input parameters for the model are listed in Table 1.

The simulated rock possesses the mechanical properties of Indiana limestone, which is mainly composed of calcite (98%); thus, the bulk modulus of the solid part was determined to be 74 GPa (Hart & Wang 1995). Fluid A and Fluid C resemble water and supercritical CO_2, respectively; Fluid B is an artificial fluid with a property between these end members, which may be considered a mixture of A and C. Even a multiphase (or two phase) flow condition is beyond the scope of this paper, we expect this fluid can provide further understanding of the behavior of intermediate fluids (between water and supercritical CO_2-like fluid) on the pore pressure distribution and fracture propagation.

Three parameters are required in Abaqus to represent a pore fluid: specific weight (density), bulk modulus and viscosity. For supercritical CO_2, these parameters will vary with temperature and pressure (Law & Bachu 1996; Span & Wagner 1996). The bulk modulus (0.058 GPa) and density (660 kg m^{-3}) of CO_2 in its supercritical condition (>7.4 MPa and >31.1°C) are much smaller than that of water under similar conditions. Such a temperature and pressure condition generally implies a minimum depth of 800 m to 1000 m in a sedimentary basin. Thus, an initial in-situ stress appropriate to a depth of about 900 m is used here, with the intermediate stress estimated on the basis of the weight of the overburden. The in-situ stress regime is typically a strike-slip regime ($\sigma_H > \sigma_v > \sigma_h$) for a cratonic basin such as the Williston basin or the Illinois basin (Zoback & Zoback 1980). Fractures in such basins at great depths are generally developed vertically and perpendicular to the minimum stress (Begnaud & Claiborne 1985), in which a plane strain condition may apply (or at least to some degree). Knowledge of the in-situ stress field is important, as the propagation axes of subsurface hydraulic fractures can be predicted on this basis (Bell & Grasby 2011).

Hydraulically induced fractures may be more likely to involve multiphase flows, with the injected fluid different from the in-situ pore fluid. To avoid the difficulty of handling a multiphase flow problem, we only consider cases with injected fluid similar to the in-situ pore fluid. In fact, the in-situ fluid and injected fluid will tend to become more alike after a period of injection, especially in the region close to the injection well. The normal traction and shear tractions in the cohesive zone were assigned to be 7.0 GPa and 8.0 GPa for all cases. The injection rate was kept at 1.50×10^{-4} m^3 s^{-1} and the injection time lasted for a total of 450 seconds.

Other parameters influenced by fluid properties are hydraulic conductivity and leak-off coefficient. Hydraulic fracture propagation behavior is very sensitive to these two parameters. To evaluate the importance of fluid compressibility (or fluid bulk modulus), hydraulic conductivity and leak-off coefficient, we conduct two phases of tests. In the Phase 1 test, hydraulic conductivity and leak-off coefficient are assigned similar values for all the three cases; thus the fracture propagation behavior will be mainly influenced by the fluid compressibility. We further assume that the permeable layers adjacent to fracture boundaries and the porous formation have the same hydraulic characteristics with respect to all fluids.

In the Phase 2 test, the effects of viscosity on hydraulic conductivity and leak-off coefficient are taken into account. Differences due to the nature of the different fluids are fully captured at this stage. Assuming the intrinsic permeability of the rock is the same for all the cases, the hydraulic conductivities k to the fluids are related by: $k_A\mu_A/\rho_A = k_B\mu_B/\rho_B = k_C\mu_C/\rho_C$. Therefore, the hydraulic conductivities assigned to each fluid are proportioned based on these relationships. The fluid leak-off coefficient

Table 1 Input parameters for the numerical model.

Rock properties			
Variable			Value
Density (kg m^{-3}) ρ			2600
Young's modulus (GPa) E			33
Poisson ratio ν			0.26
Grain bulk modulus (GPa) K_s			74
Void ratio e ($e = n/(1-n)$, n is porosity)			0.14
Pore fluid properties			
Variable	Fluid A	Fluid B	Fluid C
Density (kg m^{-3}) ρ_f	1000	880	660
Bulk modulus (GPa) K_f	2.2	0.22	0.058
Viscosity (cp) μ	1.0	0.30	0.06
Phase 1			
Hydraulic conductivity (m s^{-1}) k	2.40E-8	2.40E-8	2.40E-8
Leak-off coefficient (m s^{-1}) C	5.80E-10	5.80E-10	5.80E-10
Phase 2			
Hydraulic conductivity (m s^{-1}) k	2.18E-8	6.40E-8	2.40E-7
Leak-off coefficient (m s^{-1}) C	5.80E-10	1.93E-9	9.67E-9
In-situ stress field			
Maximum, σ_H (MPa) (x-axis)			23.8
Intermediate, σ_v (MPa) (z-axis)			21.8
Minimum, σ_h (MPa) (y-axis)			17.8
Field pore pressure (MPa)			8.8

is a very complicated parameter that is influenced by fluid viscosity, hydraulic conductivity, diffusivity, and even time (Warpinski 1991). Here, it is assumed that the leak-off coefficient is inversely proportional to the viscosity, instead of being a complicated function involving higher powers of the viscosity as in Eqn. 1, based on the assumption that the intrinsic permeability of the cohesive zone is the same for all the cases. Thus, the results can be considered as relatively conservative in the sense that the differences in behavior for different fluids are less than they could be. The input parameters for Fluid A are almost the same for Phase 1 and Phase 2, establishing a bridge for comparison between these two phases.

Phase 1 test results

Figure 6 shows the contour maps of pore pressure changes after fluid injection for all three cases of the Phase 1 test. The impacts of fluid composition on the pore pressure fields are obvious. In each case, a region of pore pressure decline occurs ahead of the fracture tip, indicating rock dilation immediately before fracturing. The simulation using pore Fluid A (water) shows a much larger pressure disturbance than that with Fluid C (supercritical CO_2) in terms of both magnitude and areal extent; Fluid B is intermediate.

Figure 7 shows pore pressure along the upper boundary of the created fracture; the lower boundary would be the same because of the symmetry. Pore pressure increases over time for all three cases. However, case A shows a much higher pore pressure level than B and C for all time steps. The pore pressures drop below the field pore pressure (88 MPa) at the fracture tip regions but finally converge to that pressure for all three cases. The regions of pore pressure decline correspond to rock dilations, and case A has the highest level of rock dilation.

Figure 8 shows the accumulated fluid leak-off volume for all three cases, and the results reveal that more compressive fluids (Fluid C) leak off more readily than less compressive fluids. The leak-off potential for fluid with a larger bulk modulus (such as Fluid A) is considerably lower, even when a higher pore pressure gradient exists in the field.

Figures 9–11 show fracture propagation curves for all three Phase 1 cases. The fracture lengths grow with injection time for each case; however, the fracture openings increase only at earlier times and then tend to stabilize or even experience a minor reduction at large injection times. These phenomena are more obvious for thin fluids, such as Fluids B and C. Fracture tip advancing rates are almost constant for Fluid A and B, but show a gradual slowing trend for the very thin fluid (Fluid C).

Figure 12 shows the fracture opening curves as measured along the upper boundaries for all three cases at the end of the simulation period (t = 450 s). The fracture

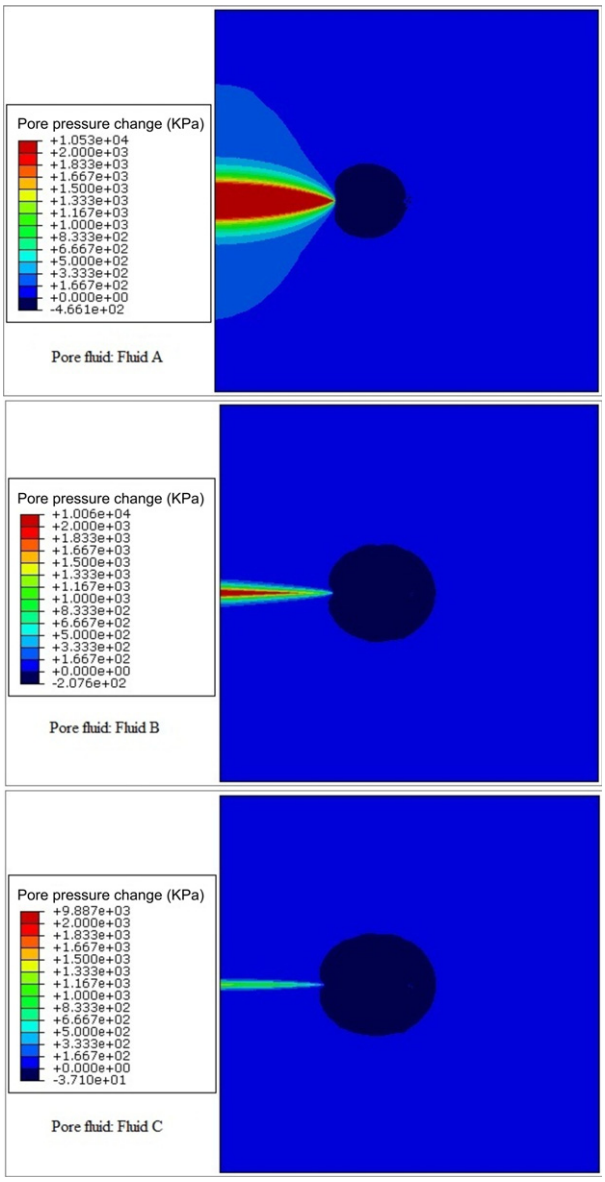

Fig. 6. Contour maps of simulated pore pressure changes after fluid injection for a similar injection rate and period for three different pore fluids (Phase 1 test).

associated with Fluid A has the largest crack opening and the longest propagation path under a similar injection flow rate and time (thus total injection quantity). Because less fluid has leaked off into the surrounding formation from the fracture for case A, more fluid is retained within the fracture to create a thicker and larger fracture. Over time, this differential behavior would become even more pronounced.

Phase 2 test results

The effect of fluid viscosity on hydraulic conductivity and leak-off coefficient are also taken into account in the Phase

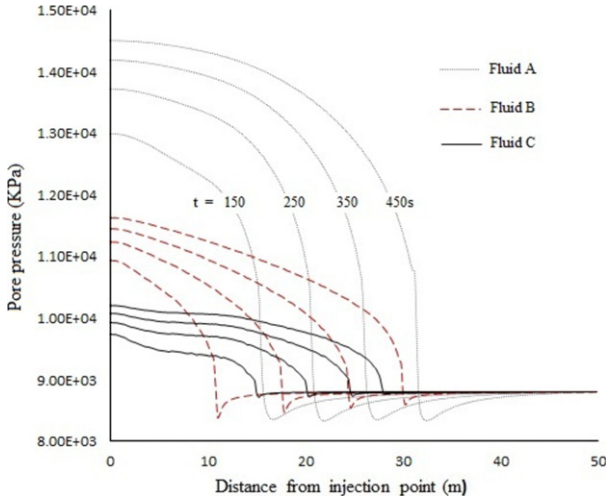

Fig. 7. Pore pressure measured along the upper boundary of the fracture (Phase 1 test).

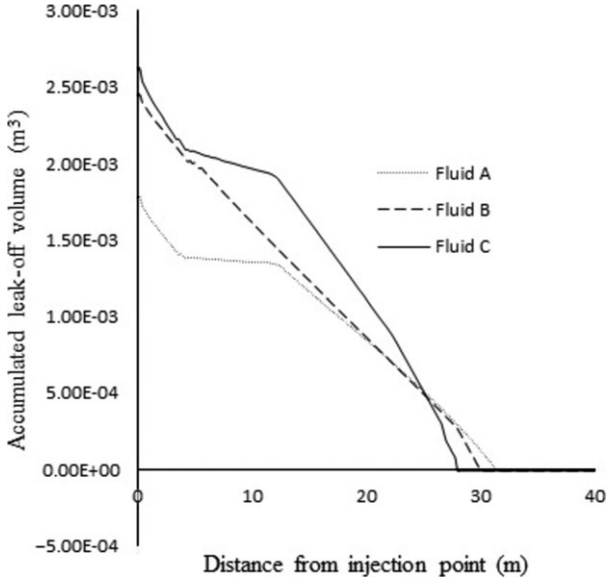

Fig. 8. Accumulated fluid leak-off volume for all cases (Phase 1 test).

2 test. Thus, Fluid C differs more from Fluid A, and the difference approaches the actual difference between water and supercritical CO_2. Figure 13 shows the contour maps of pore pressure changes after fluid injection for all three cases for the Phase 2 test. The impacts of pore fluids on the pressure fields are even more pronounced (Compare with Fig. 6). The differences in terms of fracture length are large, particularly for Fluid C, which exhibits an extremely short fracture. In addition, the rock dilation regions differ, especially in the case of Fluid C.

Figure 14 shows pore pressure measured along the upper boundary of the created fractures. The pore pressure behaviors depicted in this figure are very different from

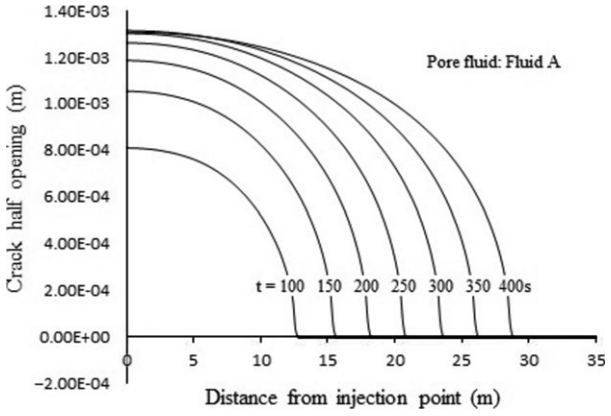

Fig. 9. Fracture propagation curves at quasi-static stages for Fluid A at different times (Phase 1 test).

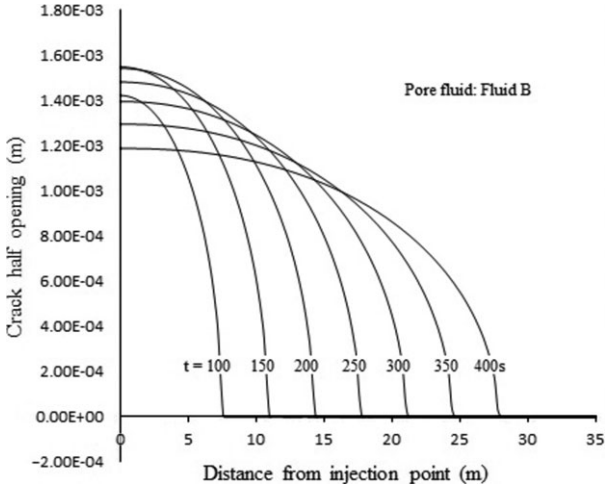

Fig. 10. Fracture propagation curves at quasi-static stages for Fluid B at different times (Phase 1 test).

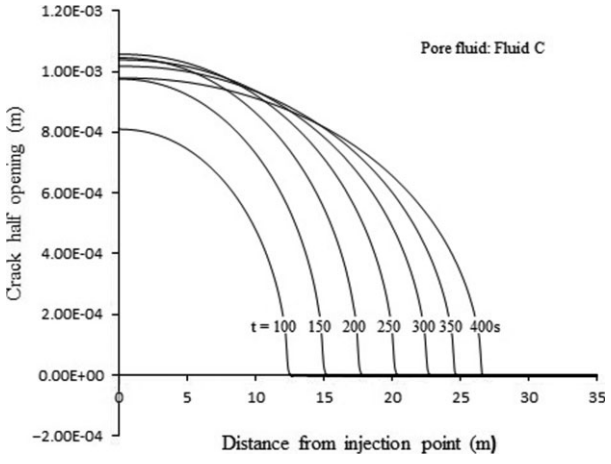

Fig. 11. Fracture propagation curves at quasi-static stages for Fluid C at different times (Phase 1 test).

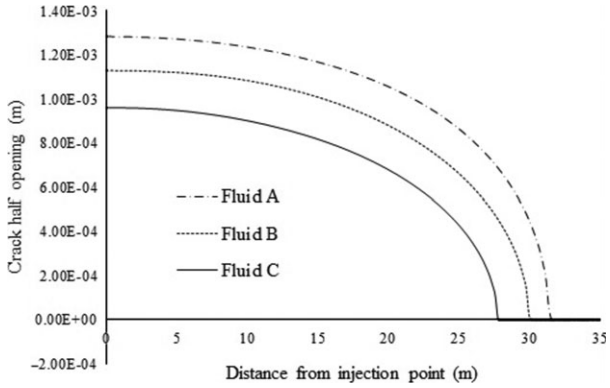

Fig. 12. Fracture opening curve as measured along upper boundaries for all the cases (Phase 1 test).

those of Figure 7, particularly for Fluids B and C. Curves for case C and case B at late times are clustered, indicating the stagnation of fracturing for these fluids.

Figure 15 shows accumulated fluid leak-off volumes for all the three cases for the Phase 2 test and reveals extremely large differences in leak-off conditions. The fracture associated with Fluid C is very short, while the leak-off is very high; and fracture associated with Fluid A is very long, while the leak-off is very low. The curves in Fig. 8 are all similar to the curve for Fluid A in Fig. 15, and the differences seen in Fig. 8 are minor in comparison to those between Figs 8 and 15. The fracture associated with Fluid C is clearly in a leak-off dominated regime. The effects of fluid viscosity are much stronger than those of fluid compressibility and can even mask the effects of the latter if tests were not conducted in two separate phases.

Figure 16 shows fracture propagation curves for all three cases for times from 50 s to 450 s. The fracture propagation behaviors associated with different fluids are very different in terms of fracture lengths, openings and propagation rates. To capture the fracture propagation behavior more clearly, Fig. 17 shows the changes of fracture lengths and openings over time.

For all three cases, both fracture lengths and openings increased during early time. This phenomenon has also been demonstrated by previous work (e.g., Bunger *et al.* 2005; Chen *et al.* 2009; Chen 2012). However, a fracture in a porous medium cannot be continuously propagated by an injection of a constant flow rate, nor can it be continuously opened by constant injection. A balancing point is reached in which the incoming fluids are completely leaked off into the adjacent porous medium, so that no fluid is left to propagate the fracture further. This phenomenon may not be captured if the test is too short and/or the domain is not large enough. There are actually two key time points; one at which a fracture ceases opening and the other at which a fracture stops extending. For all the cases simulated here, the fracture opening stops before

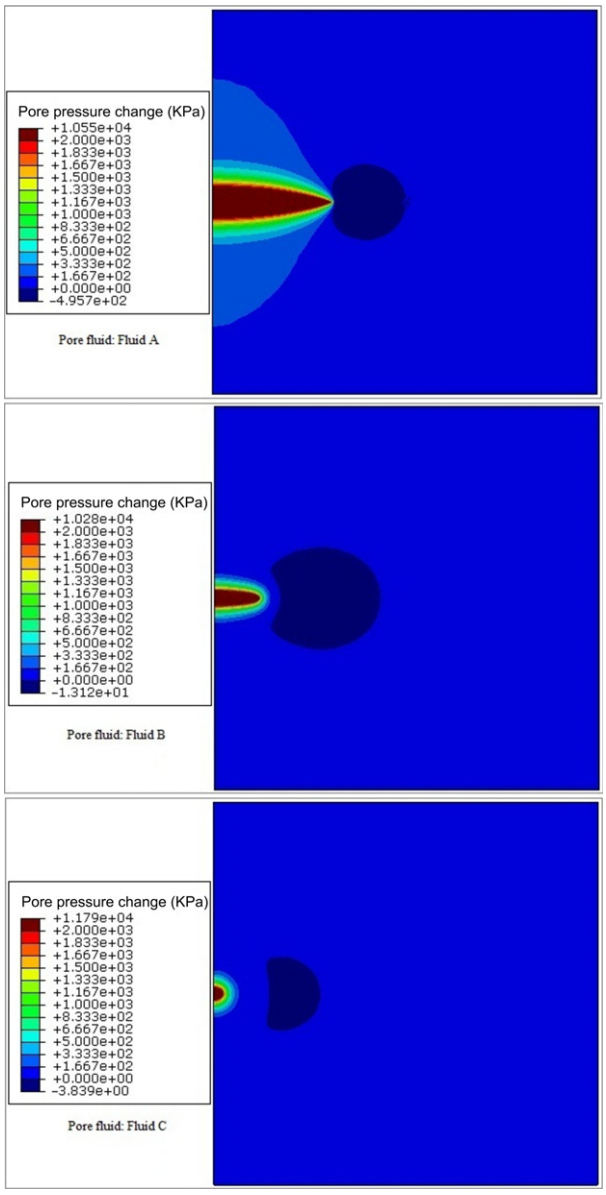

Fig. 13. Contour maps of pore pressure changes after fluid injection for three different fluids under a similar injection rate and period (Phase 2 test).

fracture propagation. Fracture propagation rates are very different for all the cases, with much slower rates for thin fluids.

In the Phase 1 test, the time at which fracture opening ceases was reached for all three cases, but the time at which fracture propagation ends was not reached for any of the cases. In the Phase 2 test, the time at which fracture opening ceases was reached for all three cases, and the time at which fracture propagation ends was reached for cases B and C, but not for A. The fracture stops opening at very early times for thin fluids (50 s for Fluid C) and fracture propagation stops after 100s, with only a minor fluctuation of fracture openings at large times. For Fluid B, the

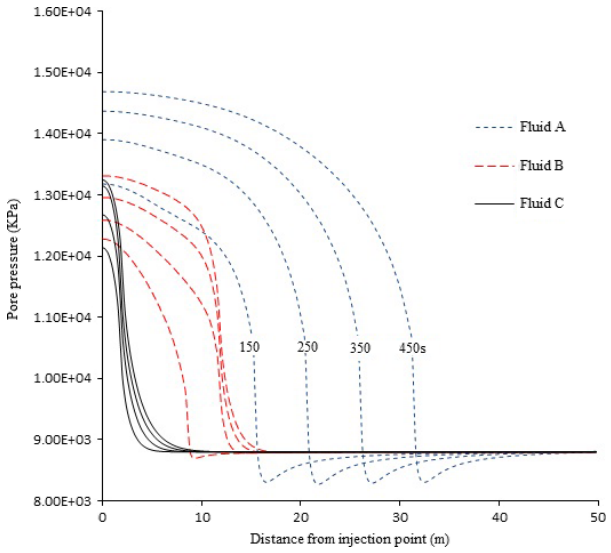

Fig. 14. Pore pressures measured along the upper boundary of the fracture (Phase 2 test).

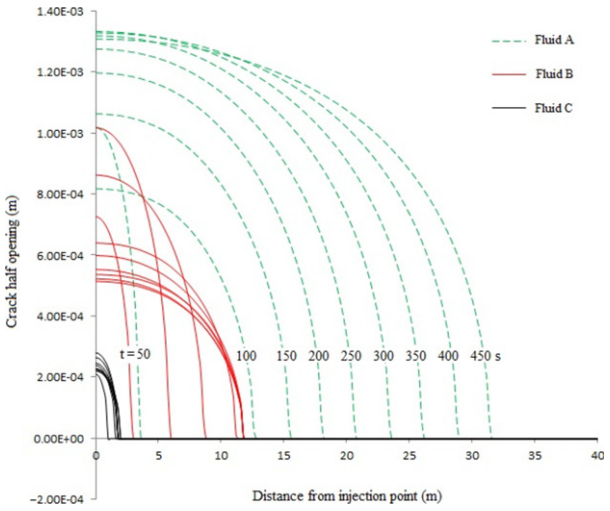

Fig. 16. Fracture opening curves as measured along upper boundary for all three cases at different times (Phase 2 test).

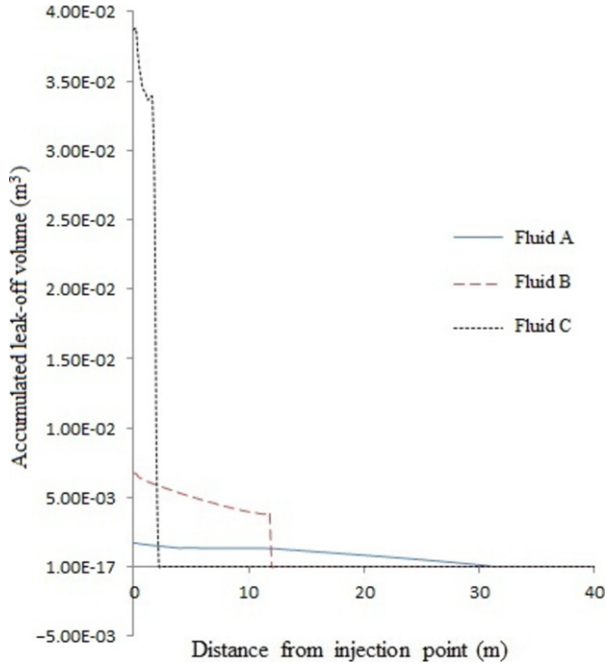

Fig. 15. Accumulated fluid leak-off volume for all the cases (Phase 2 test).

fracture stops opening after about 100s and stops propagating after about 200s. For a relatively thick fluid, such as Fluid A, the time at which the fracture ceases to open is about 300s, but the time at which fracture propagation ceases was not reached within 450s.

DISCUSSION AND CONCLUDING REMARKS

The crust behaves not as a dry medium but as a multiphase fluid-saturated porous medium (Roeloffs 1996). Fluid-

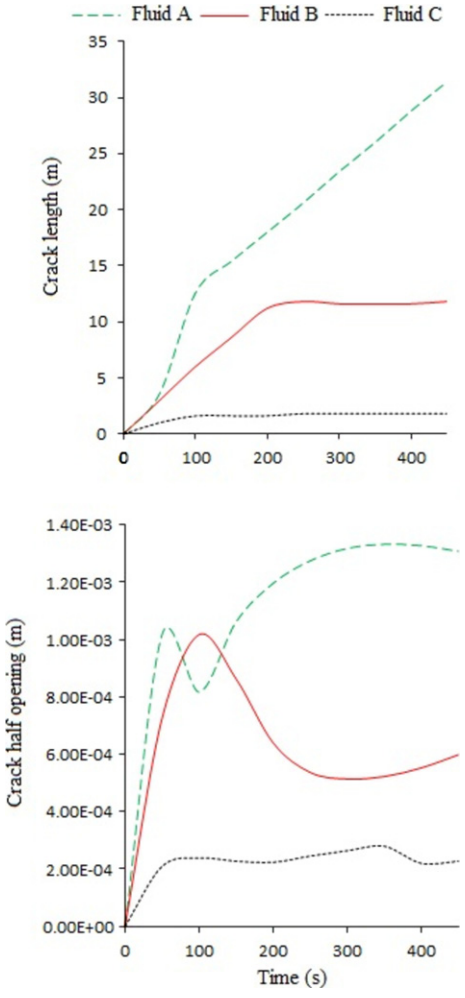

Fig. 17. Fracture length and opening as a function of time (Phase 2 test).

induced fracture propagation is essentially a problem of fluid–structure interaction. The type of fluid is important not only because the fluid that must fracture the rock, but also because rocks saturated with different pore fluids behave differently (Zhou & Burbey 2012). Therefore, when modeling the hydraulic fracturing process, one must account for the mechanics of the various fluids, as well as the mechanics of the rock, and their interaction (Sousa *et al.* 1993).

Hydraulically induced fractures are controlled to a large degree by the depth of penetration of the fracture system. Loss of fluid to the formation adjacent the fracture governs the fracture extent, which depends on the fluid viscosity and the permeability of the formation relative to the fracturing fluid, wall-building properties, and compressibility of the reservoir fluid (Howard & Fast 1957). The wall-building is envisioned as a continuous buildup of a thin layer (the filter cake) which manifests an ever increasing resistance to flow through the fracture face during fluid injection (Valko & Ecomomides 1995). Effective stress field variations due to fluid injection depend on diffusion through the poroelastic rock mass as well as diffusion in preferential directions or through fresh shear zones or other hydraulically induced fractures (Cornet 2012).

Crack openings are essentially controlled by fluid pressure declines in the fracture, as well as fluid leak-off potential if the formation is porous. Operating conditions which cause high pressure declines along the crack (such as a high injection rate and highly viscous fluids) will result in relatively wide cracks. Conversely, conditions that cause low pressure declines (low injection rates and thin fluids) will result in relatively narrow cracks (Perkins & Kern 1961). Decreased viscosity can lead to undesirable flow characteristics. It has been shown that the use of a non-Newtonian hydraulic fracturing fluid may change the velocity of hydraulic fracture crack propagation (Tagirova 2009). The opening of a fracture is a transient phenomenon and undrained conditions apply, that is, the injected fluid will 'instantly' occupy the entire fracture and we can expect 100% saturation of a thin fracture with the injected fluid if this fracture is freshly initiated.

We studied the influence of fluid properties on fracture propagation behavior by using the cohesive zone model in conjunction with a poroelasticity model. We simulate fracture propagation due to the effects of a thin fluid having the properties of supercritical CO_2 by conducting two phases of numerical tests, with a normal fluid (water) as the basis for comparison. Our findings can be summarized as follows:

(1) A pore fluid is characterized in terms of its compressibility and viscosity, and both of these parameters have impacts on the behavior of fracture propagation. However, fluid viscosity is the most significant property, as it greatly affects the hydraulic conductivity and leak-off coefficient. The effect of viscosity can dominate and mask the effect of compressibility in numerical tests.
(2) Relatively large time periods and spatial domains are required to capture the hydraulically induced fracture propagation behavior. Two important times have been identified during a fracturing process in a porous medium: the time at which a crack ceases to open further, and the time at which a crack ceases propagating, with the former occurring before the latter for all tested cases.
(3) The pore pressure fields are very different for different fluids even when the initial field conditions and injection schemes (rate and time) are the same. Thin fluids will create thinner and much shorter fractures relative to thick fluids. This agrees with laboratory observations that viscous fluids tend to generate thick cracks and thin fluids tend to generate thin cracks. This result agrees with field observations that injected CO_2 may not even fracture the formation if the injection rate is not high enough.
(4) Crack propagation rates associated with thick fluids are much higher than those associated with thin fluids, and these rates can only be considered constant within intermediate time ranges. The rate is a quasi-logarithmic type function of time, with an initial sharp increase followed by level-off at large times. The crack width can fluctuate after the initial opening stage, and the opening of a fracture by a thin fluid tends to be less stable than one created by a thick fluid.

Fluid properties have significant impact on the behavior of fracture propagation in porous media, and the differences in fracture opening and propagation associated with different fluids can be extremely large. The very short fractures associated with thin fluids do not necessarily mean that the fracturing is inconsequential, because the rock dilation region is far from the crack tip (Fig. 13). This suggests that an abnormal pressure front can advance far ahead of an obvious crack. The actual fractures created by thin fluids can be extremely narrow. Further research is needed in this area, as the impact of fluid properties is also complicated by chemo-thermo-hydro-mechanical coupling.

ACKNOWLEDGEMENTS

This technical effort was performed in support of the National Energy Technology Laboratory's ongoing research in geologic CO_2 sequestration under the RES contract DE-FE0004000. Two anonymous reviewers and the editor are greatly appreciated for providing very helpful comments. Any opinions, findings, and conclusions expressed in this material are those of the authors and do not necessarily state or reflect the views of the US Government or any agency thereof.

NOMENCLATURE

C	diffusivity coefficient
e	void ratio of rock formation ($e = n/(1\text{-}n)$)
h	hydraulic head
l	fracture length as measured from injection point to fracture tip
k	hydraulic conductivity
$m_f/\Delta m_f$	fluid mass/fluid mass change
n	porosity of rock formation
p_∞	field pore pressure: pore pressure with enough distance from the fracture thus can be considered as a reference state without the disturbance of fluid injection.
p_b	pore pressure on the fracture boundary
p_c	pore pressure on the fracture center line
p_i	fluid injection pressure
q	fracturing fluid flow inside the fracture
q_T	fracturing fluid tangential flow inside the fracture
q_N	fracturing fluid normal flow inside the fracture
t/t_0	time/lapse time since the exposure of the fracture surface to the fluid
t_n/t_s	normal traction/shear traction
v_l	Leak-off velocity
$w/w(x,t)$	fracture aperture/aperture as a function of position and time during fluid injection
B	Skempton's B coefficient (the ratio of the induced pore pressure to the change in confining stress under undrained condition)
C/C'	leak-off coefficient/dimensionless leak-off coefficient
E	Young's modulus (stiffness of rock)
E'	dimensionless Young's modulus
G	shear modulus (the ratio of shear stress to shear strain)
G_c	cohesive energy
K'	dimensionless toughness
K_{IC}	fracture toughness (resistance offered by material against crack propagation)
K	bulk modulus (the ratio of stress and volumetric strain at constant pore pressure, and $1/K$ is the compressibility of the material)
K_s	solid grain's bulk modulus (the ratio of confining stress and volumetric strain, $K_s = K$ for material without pores)
$1/K_n$	unjacketed pore compressibility (K_n: the unjacketed pore bulk modulus) (change in pore volume over pore pressure change with confining pressure required to track with the pore pressure)
K_f	pore fluid bulk modulus (definition is the same to K but with respect to fluid)
$Q(t)\delta(x,y)$	local fluid flux in a fracture
Q_0	injection rate
S_s	specific storage coefficient (a correlation between stored fluid mass and pore pressure).
T/T_{max}	traction tensor/the maximum
V_{inject}	injected fluid volume
V_{inject}	volume of the injected fluid stored in the crack
V_{leak}	volume of the injected fluid leaked into the porous formation
α	compressibility of the formation along the vertical direction.
δ_{ij}	Kronecker delta
ε_{ij}	strain tensor
η	an intermediate poroelastic parameter as defined by Eqn. 13.
κ	intrinsic permeability
μ	fluid viscosity
v/v_u	drained Poisson's ratio/undrained Poisson's ratio
ρ	bulk density
ρ_f	fluid density
σ_0/σ_{ij}	confining stress/confining stress tensor
ψ	cohesive potential function
Ω/Ω_f	displacement jump across a pair of cohesive surfaces/the critical separation at complete failure of cohesive zone

REFERENCES

Abousleiman YN (1991) A poroelastic PKN model with pressure dependent leakoff and formation permeability determination. PhD. Dissertation, University of Delaware.

Adachi JI (2001) Fluid-driven fracture in permeable rock. PhD. Dissertation, University of Minnesota, Minneapolis.

Adachi JI, Detournay E (2008) Plane strain propagation of a hydraulic fracture in a permeable rock. *Engineering Fracture Mechanics*, **75**, 4666–94.

Adachi JI, Siebrits E, Peirce A, Desroches J (2007) Computer simulation of hydraulic fractures. *International Journal of Rock Mechanics and Mining Science*, **44**, 739–57.

Barenblatt GI (1959) The formation of equilibrium cracks during brittle fracture: general ideas and hypothesis, axially symmetric cracks. *Journal of Applied Mathematics and Mechanics*, **23**, 622–36.

Barenblatt GI (1962) The mathematical theory of equilibrium cracks in brittle fracture. *Advances in Applied Mechanics*, **7**, 55–129.

Begnaud WJ, Claiborne EB Jr (1985) Vertical fracture growth considerations in the Mission Canyon/Radcliffe Formations of the North Alexander area. SPE 14375. 60th Annual Tech. Conf. SPE, Las Vegas, NV, Sep. 22-25.

Bell JS, Grasby SE (2011) The stress regime of the Western Canadian Sedimentary Basin. *Geofluids*, **12**, 150–65.

Berryman JG (2012) Poroelastic response of orthotropic fractured porous media. *Transport in Porous Media*, **93**, 293–307.

Berryman JG, Milton GW (1991) Exact results for generalized Gassmann's equations in composite porous media with two constituents. *Geophysics*, **56**, 1950–60.

Boone TJ, Ingraffea AR (1990) A numerical procedure for simulation of hydraulically driven fracture propagation in

poroelastic media. *International Journal for Numerical and Analytical Methods in Geomechanics*, **14**, 27–47.
Boone TJ, Wawrzynek PA, Ingraffea AR (1986) Simulation of fracture process in rock with application to hydrofracturing. *International Journal of Rock Mechanics and Mining Sciences & Geomechanics Abstracts*, **23**, 255–65.
Bunger AP, Detournay E (2008) Experimental validation of the tip asymptotics for a fluid-driven crack. *Journal of the Mechanics and Physics of Solids*, **56**, 3101–15.
Bunger AP, Detournay E, Garagash DI (2005) Toughness-dominated hydraulic fracture with leak-off. *International Journal of Fracture*, **134**, 175–90.
Camacho GT, Ortiz M (1996) Computational modeling of impact damage in brittle materials. *International Journal of Solids and Structures*, **33**, 2899–938.
Carrier B, Granet S (2012) Numerical modeling of hydraulic fracture problem in permeable medium using cohesive zone model. *Engineering Fracture Mechanics*, **79**, 312–28.
Chen ZR (2012) Finite element modelling of viscosity-dominated hydraulic fractures. *Journal of Petroleum Science and Engineering*, **88–89**, 136–44.
Chen ZR, Bunger AP, Zhang X, Jeffrey RG (2009) Cohesive zone finite element based modeling of hydraulic fractures. *Acta Mechanica Solida Sinica*, **22**, 443–52.
Cheng AH-D, Detournay E (1998) On singular integral equations and fundamental solutions of poroelasticity. *International Journal of Solids and Structures*, **35**, 4521–55.
Cheng AH-D, Abousleiman Y, Roegiers IC (1993) Review of some poroelastic effects in rock mechanics. *International Journal of Rock Mechanics and Mining Sciences*, **30**, 1119–26.
Cornet FH (2012) The relationship between seismic and aseismic motions induced by forced fluid injections. *Hydrogeology Journal*, **20**, 1463–6.
Detournay E (2004) Propagation regimes of fluid-driven fractures in impermeable rocks. *International Journal of Geomechanics*, **4**, 35–45.
Detournay E, Cheng A-D (1991) Plane strain analysis of a stationary hydraulic fracture in a poroelastic medium. *International Journal of Solids and Structures*, **27**, 1645–62.
Detournay E, Cheng A-D, McLennan TD (1990) A poroelastic PKR hydraulic fracture model based on an explicit moving algorithm. *ASME Journal of Energy Resource Technology*, **112**, 224–30.
Dugdale DS (1960) Yielding of steel sheets containing slits. *Journal of the Mechanics and Physics of Solids*, **8**, 100–4.
Economides MJ, Nolte KG (2000) *Reservoir Stimulation*, 3rd edn, John Wiley & Sons, Chichester, UK.
Elices M, Guinea GV, Gomez J, Planas J (2002) The cohesive zone model: advantages, limitations and challenges. *Engineering Fracture Mechanics*, **69**, 137–63.
Evans KF, Cornet FH, Hashida T, Hayashi K, Ito T, Matsuki K (1999) Stress and rock mechanics issues of relevance to HDR/HWR engineered geothermal systems: review of developments during the past 15 years. *Geothermics*, **28**, 455–74.
Falk MA, Needleman A, Rice JR (2001) A critical evaluation of dynamic fracture simulations using cohesive surfaces. *Journal de Physique IV*, **11**, 43–52.
Fenghour A, Wakeham WA, Vesovic V (1998) The viscosity of carbon dioxide. *Journal of Physical and Chemical Reference Data*, **27**, 31–44. doi:10.1063/1.556013.
Fink JK (2011) *Petroleum Engineer's Guide to Oil Field Chemicals and Fluids*. Elsevier, Waltham, MA, USA.
Frank U, Barkley N (2005) Remediation of low permeability subsurface formations by fracturing enhancements of soil vapor extraction. *Journal of Hazardous Materials*, **40**, 191–201.
Garagash DI (2006) Plane-strain propagation of a fluid-driven fracture during injection and shut-in: Asymptotics of large toughness. *Engineering Fracture Mechanics*, **74**, 456–81.
Geertsma J, de Klerk F (1969) A rapid method of predicting width and extent of hydraulically induced fractures. *Journal of Petroleum Technology*, **21**, 1571–81.
Green DH, Wang HF (1990) Specific storage as a poroelastic coefficient. *Water Resource Research*, **26**, 1631–7.
Haimson BC, Cornet FH (2003) ISRM suggested methods for rock stress estimation – Part 3: hydraulic fracturing (HF) and/or hydraulic testing of pre-existing fractures (HTPF). *International Journal of Rock Mechanics and Mining Sciences*, **40**, 1011–20.
Haimson BC, Fairhurst C (1969) Hydraulic fracturing in porous permeable materials. *Journal of Petroleum Technology*, **21**, 811–7.
Harris PC, Haynes RJ, Egger JP (1984) The use of CO_2-based fracturing fluids in the Red Fork Formation in the Anadarko Basin, Oklahoma. *Journal of Petroleum Technology*, **36**, 1003–8.
Hart DJ, Wang HF (1995) Laboratory measurements of a complete set of poroelastic moduli for Berea sandstone and Indiana limestone. *Journal of Geophysical Research*, **100(B9)**, 17741–51.
Heidaryana E, Hatamib T, Rahimib M, Moghadasi J (2011) Viscosity of pure carbon dioxide at supercritical region: measurement and correlation approach. *The Journal of Supercritical Fluids*, **56**, 144–51.
Hibbitt, Karlsson & Sorensen, Inc. (1998) *ABAQUS, Standard User's Manual*, Hibbitt, Karlsson & Sorensen, Inc., Pawtucket, Rhode Island.
Hillerborg A, Modeer M, Petersson PE (1976) Analysis of crack formation and crack growth in concrete by means of fracture mechanics and finite elements. *Cement and Concrete Research*, **6**, 773–82.
Howard GC, Fast CR (1957) Optimum fluid characteristic for fracture extension. *Drilling and Production Practice*, **24**, 261–70.
Ishida T, Chen Q, Mizuta Y, Roegiers J-C (1998) Influence of fluid viscosity on hydraulically induced crack geometry. *International Journal of Rock Mechanics and Mining Sciences*, **35**, 460–2.
Ishida T, Chen Q, Mizuta Y, Roegiers J-C (2004) Influence of fluid viscosity on the hydraulic fracturing mechanism. *Journal of Energy Resources Technology*, **126**, 190–200. doi:10.1115/1.1791651.
Ishida T, Aoyagi K, Niwa T, Chen Y, Murata S, Chen Q, Nakayama Y (2012) Acoustic emission monitoring of hydraulic fracturing laboratory experiment with supercritical and liquid CO_2. *Geophysical Research Letters*, **39**, 1–6.
Law DHS, Bachu S (1996) Hydrogeological and numerical analysis of CO_2 disposal in deep aquifers in the Alberta sedimentary basin. *Energy Conversion and Management*, **37**, 1167–74.
Legarth B, Huenges E, Zimmermann G (2005) Hydraulic fracturing in sedimentary geothermal reservoir: results and implications. *International Journal of Rock Mechanics and Mining Sciences*, **42**, 1028–41.
Murdoch LC, Slack WW (2002) Forms of hydraulic fractures in shallow fine-grained formations. *Journal of Geotechnical and Geoenvironmental Engineering*, **128**, 479–87.
Needleman A (1987) A continuum model for void nucleation by inclusion debonding. *ASME Journal of Applied Mechanics*, **54**, 525–31.

Papanastasiou P (1999) The effective fracture toughness in hydraulic fracturing. *International Journal of Fracture*, **96**, 127–47.

Papanastasiou P, Thiercelin M (1993) Influence of inelastic rock behavior in hydraulic fracturing. *International Journal of Rock Mechanics and Mining Sciences & Geomechanics Abstracts*, **30**, 1241–7.

Peirce A, Detournay E (2008a) An implicit level set method for modeling hydraulically driven fractures. *Computer Methods in Applied Mechanics and Engineering*, **197**, 2858–85.

Peirce A, Detournay E (2008b) An Eulerian moving front algorithm with weak-form tip asymptotics for modeling hydraulically driven fractures. *Communications in Numerical Methods in Engineering*, **25**, 185–200.

Perkins TK, Kern LR (1961) Widths of hydraulic fractures. *Journal of Petroleum Technology*, **13**, 937–49.

Pinder GF, Gray WG (2008) *Essentials of Multiphase Flow and Transport in Porous Media*. John Wiley & Sons, Inc., New Jersey, USA.

Pollard DD (1976) On the form and stability of open hydraulic fractures in the earth's crust. *Geophysical Research Letters*, **3**, 513–6.

Renshaw CE, Harvey CF (1994) Propagation velocity of a natural hydraulic fracture in a poroelastic medium. *Journal of Geophysical Research*, **99**, 21667–77.

Rice JR, Cleary MP (1976) Some basic stress diffusion solutions for fluid-saturated porous media with compressible constituents. *Reviews of Geophysics*, **14**, 227–41.

Roeloffs E (1996) Poroelastic techniques in the study of earthquake-related hydrologic phenomena. *Advances in Geophysics*, **37**, 135–95.

Sarris E, Papanastasiou P (2011) The influence of the cohesive process zone in hydraulic fracturing modeling. *International Journal of Fracture*, **167**, 33–45.

Savitski A, Detournay E (2002) Propagation of a fluid-driven penny-shaped fracture in an impermeable rock: asymptotic solutions. *International Journal of Solids and Structures*, **39**, 6311–37.

Schoenball M, Muller TM, Muller BIR, Heidbach O (2010) Fluid-induced micro-seismicity in pre-stressed rock masses. *Geophysical Journal International*, **180**, 813–9.

Shet C, Chandra N (2002) Analysis of energy balance when using cohesive zone models to simulate fracture processes. *Journal of Engineering Materials and Technology -Transactions of the ASME*, **124**, 440–50.

Sinal ML, Lancaster G (1987) Liquid CO_2 fracturing: advantages and limitations. *Journal of Canadian Petroleum Technology*, **26**, 26–30.

Sousa J, Carter B, Ingraffea A (1993) Numerical simulation of 3D hydraulic fracture using Newtonian and power-law fluids. *International Journal of Rock Mechanics and Mining Sciences*, **30**, 1265–71.

Span R, Wagner W (1996) A new equation of state for carbon dioxide covering the fluid region from the triple-point to 1100 K at pressures up to 88 MPa. *Journal of Physical and Chemical Reference Data*, **25**, 1509–96.

Spence DA, Sharp P (1985) Self-similar solutions for elastohydrodynamic cavity flow. *Proceedings of the Royal Society London*, **A400**, 289–313.

Spence DA, Turcotte DL (1985) Magma driven propagation of cracks. *Journal of Geophysical Research*, **90(B1)** 575–80.

Sun RJ (1969) Theoretical size of hydraulically induced horizontal fractures and corresponding surface uplift in an idealized medium. *Journal of Geophysical Research*, **74**, 5995–6011.

Tagirova VR (2009) Hydraulic fracture crack propagation driven by a non-Newtonian fluid. *Moscow University Mechanics Bulletin*, **64**, 135–42.

Tomar V, Zhai J, Zhou M (2004) Bounds for element size in a variable stiffness cohesive finite element model. *International Journal for Numerical Methods in Engineering*, **61**, 1894–920.

Valko P, Ecomomides MJ (1995) *Hydraulic Fracture Mechanics*. John Wiley & Sons Ltd, West Sussex PO19 IUD, England.

Warpinski NR (1991) Hydraulic fracturing in tight, fissured media. *Journal of Petroleum Technology*, (FEB), **43**, 146–52.

Yao Y (2012) Linear elastic and cohesive fracture analysis to model hydraulic fracture in brittle and ductile rocks. *Rock Mechanics and Rock Engineering*, **45**, 375–87.

Zhou XJ, Burbey TJ (2012) A FEM approach to measure Skempton's B coefficient for supercritical CO2-saturated rock. *Environmental & Engineering Geoscience*, **18**, 343–55.

Zoback ML, Zoback MD (1980) State of stress in the conterminous United States. *Journal of Geophysical Research*, **85**, 6113–56.

Zoback MD, Rummel F, Jung R, Raleigh CB (1977) Laboratory hydraulic fracturing experiments in intact and pre-fractured rock. *International Journal of Rock Mechanics and Mining Sciences & Geomechanics Abstracts*, **14**, 49–58.

GEOFLUIDS

Volume 14, Number 2, May 2014
ISSN 1468-8115

CONTENTS

WILEY
Blackwell

Geofluids* is abstracted/indexed in *Chemical Abstracts

This journal is available online at Wiley Online Library.
Visit onlinelibrary.wiley.com to search the articles and register for table of contents and e-mail alerts.